Dendrite-free Al Recycling via Electrodeposition using Ionic Liquid Electrolytes: The Effect of Deposition Temperature and Cathode Surface Roughness

Yifan Wang, Ramana G. Reddy and Ruigang Wang*

Department of Metallurgical and Materials Engineering, The University of Alabama, Tuscaloosa, AL 35487, USA

Abstract

In this paper, the electrodeposition of Al from aluminum scrap alloys (A2020) on copper cathode substrates with varied surface roughness under different deposition temperatures was studied using low-temperature $AlCl_3$-1-butyl-3-methyl-imidazolium chloride (BMIC) ionic liquid electrolytes. The bulk electrodeposition of Al was carried out under a voltage of 1.5 V at a stirring rate of 120 rpm using a fixed ionic liquid electrolyte concentration (molar ratio $AlCl_3$: BMIC = 2:1). The effects of deposition temperature (range from 80 ºC to 140 ºC) and surface roughness of Cu cathode substrates (polished by 320, 600, 800, 1200 grits SiC sandpapers and mirror polishing process) on the morphology of deposited Al, current density, current efficiency and energy consumption, were investigated. The Al deposits were characterized using scanning electron microscopy (SEM) with energy-dispersive X-ray spectroscopy (EDS), X-ray diffraction (XRD), profilometer, and electrochemical measurements for current density, current efficiency, and energy consumption. It is demonstrated that the deposition temperature and surface roughness of Cu electrodes play a critical role in the nucleation and growth of Al deposits. Higher deposition temperature promotes the diffusion and/or migration of $Al_2Cl_7^-$ ions and then enhances the current density and efficiency during the electrodeposition of Al. Smoother surface of Cu electrodes is preferred for the formation of dendrite-free Al deposits. Typically, on the

mirror polished Cu electrode, no Al dendrite structure was observed, and only plate-like Al deposits were formed at the deposition temperature of 100 ^{o}C. Pure metallic Al was successfully deposited on Cu electrodes in $AlCl_3$+BMIC ionic liquid electrolytes for all experiments with a current efficiency range from 72 % to 99 % and energy consumption of 4.6 to 6.3 kWh/kg Al.

Keywords: Al electrodeposition; ionic liquid electrolyte; dendrite structure; deposition temperature; substrate surface roughness

*Corresponding author: rwang@eng.ua.edu (R. Wang)

1. Introduction

Aluminum (Al) and its alloys are extensively used in transportation and construction applications due to their low density (ρ_{Al}=2.7 g/cm^3), excellent ductility and recyclability, and good mechanical properties. High demand and production cost of aluminum and its alloys have driven more efficient and sustainable recycling techniques in terms of saving energy and reducing amounts of pollutant emissions. The general industrial aluminum recycling/refining processes, including Hoope's process and segregation process, require high working temperature ca. 900 ºC to 1000 ºC. These processes consume high energy (15 to 18 kWh/kg Al), and lead to significant emissions of green-house gases such as CO, CO_2, CF_4 and so on (Abbott et al., 2005).

Among many other efforts, the electrodeposition (also called electrorefining or electrorecycling) of Al from aluminum alloy scraps using ionic liquid electrolytes, which is an energy-efficient and environmentally friendly method, has attracted significant attention for recycling aluminum-containing metallic wastes in recent years. These efforts include to investigate the use of different surfactants in electrodeposition (Gomes and da Silva Pereira, 2006), the effect of overpotential on dendrite formation (Kamavaram et al., 2005), the electrochemical characterization of Al deposition (Popov et al., 1979; Zhang and Reddy, 2006a) and the effect of process variables on current efficiency (Reddy, 2006b).

However, insights into relationship between the microstructure, recycling efficiency and product purity with various processing parameters have not been sufficiently investigated or understood. For instance, according to Kuma et al's work (Kuma et al., 2019), the impurity (S and Cl) in deposited Al from $DMSO_2$-$AlCl_3$ bath leaded to the limited ductility of resultant Al electrodeposits. And the Huan et al (Huan et al., 2020) reported the recovery of aluminum from coarse Al-Si alloy, which could produce aluminum deposits with 99% purity, but the current

density was relatively low (30 mA/cm^2) at 170 ^{o}C. Recently, Yang et al (Yang et al., 2020) studied the electrodeposition of Al from $AlCl_3$-[EMIm]Cl ionic liquid (a similar ionic liquid system used in this study) at low temperature (60 ^{o}C) for the application of Li-ion battery anode, the current density was lower than 0.02 mA/cm^2, which was impractical for industrial application of Al recycling. In Addition, one of the major challenges in the current electrodeposition of Al for recycling processing is the formation of dendritic deposits, which creates one dimensional (1D) dendrite structure and remains a critical concern due to possible internal short circuits in an unpredictable manner. Dendrite is one type of nonadherent structures, which adds extra cost for further processing owing to its low density. This 1D dendritic structure decreases current density, current efficiency and prevents subsequent deposition which has a profound unfavorable effect on the deposition/recycling efficiency of Al (Pradhan et al., 2009). Another adverse outcome of forming Al dendrite structure is the difficulty to achieve the large-scale electrodeposition of aluminum scraps, while the system may not be homogenous at large scale and the large amount of ionic liquid is unstable. Therefore, in order to minimize the effects of unconstrained dendrite development, an intimate understanding of the formation of Al dendrite structures under different deposition conditions is needed.

The goal of this research is to understand the role of processing conditions on the formation mechanisms of Al dendrite deposits during the electrodeposition, to identify the critical electrodeposition parameters for dendrite-free Al deposits, and to minimize the production cost for aluminum-based alloys scrap recycling. In the present work, the effects of deposition temperature and surface roughness of Cu electrodes on the current density, current efficiency, energy consumption and morphology of the electrodeposited Al using $AlCl_3$ and BMIC mixture as ionic liquid electrolytes were investigated.

2. Experimental section

2.1 Aluminum electrodeposition

The ionic liquid electrolytes were prepared by mixing $AlCl_3$ and BMIC at a molar ratio of $AlCl_3$: BMIC = 2:1. The electrodeposition experiments were conducted in a 50-mL glass beaker fitted with Teflon cap. The Al2020 aluminum alloy scrap was used as anode material and the Cu sheet was used as cathode material. The aluminum alloy scrap (anode material) was cut into thin plate shape and polished mechanically before deposition. The applied potential was controlled by a power supply at 1.5 V and the stirring rate during deposition was 120 rpm. All experiments were protected in an argon-controlled atmosphere with the applied potential for a period of 2 h. To study the effect of deposition temperature, all Cu electrodes were polished by 320 grit SiC sandpaper and a digital hot plate combined with a thermometer was used to control the deposition temperature from 80 ^oC to 140 ^oC. To study the effect of surface roughness of Cu electrode, the deposition temperature was kept at 100 ^oC and the Cu electrodes were polished by 320, 600, 800, 1200 grits SiC sandpapers and mirror polishing procedure (with 3 μm SiO_2 fine colloidal suspension), respectively. The surface roughness profiles of Cu electrodes after different polishing treatments were collected by a KLA Tencor D500 Profilometer under 15.0 mg stylus force. The total scanning length of profiles was 1 mm and the scanning speed was 0.1 mm/sec. Each sample was scanned three times from different positions to obtain the mean surface roughness and the relative error bar. As plotted in Fig. 1, the surface roughness of polished Cu cathodes are 543.1/126.7/ 78.6/46.2/23.3 nm after polishing by 320 / 600 / 800/ 1200 grits of SiC sandpaper and mirror polishing process, respectively. These polished Cu electrodes are referred as 320G Cu, 600G Cu, 800G Cu, 1200G Cu and mirror Cu. All deposited Al samples were washed thoroughly by acetone and DI water. Finally, the samples were dried in

a vacuum oven at 50 ^{o}C for 5 h. In this study, the surface roughness of Cu electrodes was controlled by polishing using different grit size of SiC sandpapers. Similarly, other polishing or processing techniques, including ball milling, hydroabrasive grinding, grinding wheel, ultrasonic processing, and chemical and electric etching, can also be used to obtain the same or similar electrode surface roughness.

2.2 Electrochemical measurements of Al electrodeposition

Due to the Al-rich molar ratio of $AlCl_3$: BMIC = 2: 1, there are mainly $AlCl_4^-$ and $Al_2Cl_7^-$ ions in the ionic liquid electrolyte solution (Pradhan and Reddy, 2012, 2014). By applying potential between Cu cathode and Al anode, the Al anode reacts with $AlCl_4^-$ ions at the interface of Al electrode/ ionic liquid electrolyte, producing $Al_2Cl_7^-$ ions as illustrated in Eq. [1].

$$Al + 7AlCl_4^- = 4Al_2Cl_7^- + 3e^- \quad [1]$$

The reaction on Cu cathode side consumes $Al_2Cl_7^-$ ions and yields Al deposits over Cu electrode surface as shown in Eq. [2].

$$4Al_2Cl_7^- + 3e^- = Al + 7AlCl_4^- \quad [2]$$

The current density (j) is defined as the amount of charge per unit time that flows through a unit area of a chosen cross section. It is calculated by the electric current flowing through the deposited Al area on Cu electrode. Eq. [3] is used to obtain the current density (j):

$$j = \frac{I}{A} \quad [3]$$

Where I is the average current (A) obtained when the current became stable, and A is the measured covering area with Al deposits.

The current efficiency (η) is defined as the percentage of the current which goes to the useful Al electrodeposition reaction. In our case, it is determined by the percentage of the actual deposited amount of Al to the theoretically calculated amount of Al. The experimental weight

gain (Δw) of Al can be obtained by the mass difference of Cu electrode before and after the electrodeposition and cleaning processes ($\Delta w = w_{final} - w_{initial}$). The theoretical weigh gain (w_t) of Al can be calculated by using Faraday's law by Eq. 4:

$$w_t = \frac{ItM}{zF} = \frac{QM}{zF} \quad [4]$$

Where Q is the total supplied electric charge (Coulomb, $Q = I \times t \ \ or \ \ Q = \int I\,dt$), I is the current (A), t is the working time (s), M is the atomic weight of Al deposits (26.98 g/mol), z is the number of transferred electrons which is equal to 3 in this case and F is the Faraday constant (96,485 C/mol). Then the current efficiency (η) can be calculated via Eq. [5].

$$\eta = \frac{\Delta w}{w_t} \times 100\% \quad [5]$$

One of the critical components for the cost estimation of metal electrodeposition recycling is the energy consumption. The energy consumption (E) can be calculated via Eq. [6]:

$$E = \frac{VQ}{\Delta w} \quad [6]$$

Where V is the applied potential (Volt), Q is the total supplied electric charge (Coulomb, $Q = I \times t \ \ or \ \ Q = \int I\,dt$), and Δw is the experimental weigh gain of Al deposits.

2.3 XRD and SEM Characterization

The phase characteristics and crystallinity of Al deposits on Cu electrodes were analyzed using X-ray diffraction (XRD). The XRD analysis was performed using a Philips X'Pert MPD diffractometer with Cu Kα radiation (λ= 1.5418 Å) in the Bragg's angle range from 20° to 90° with a step size of 0.05°/min.

The morphology and chemical composition characterization of Al deposits were carried out using Apreo field-emission scanning electron microscope (Apreo FE-SEM, ThermoFisher

Scientific) equipped with an energy dispersive X-ray spectrometer (Bruker XFlash EDS). 5 kV and 10 kV acceleration voltages were used for SEM imaging and obtaining EDS spectrum, respectively. Both cross-section and plan-view SEM imaging were carried out to obtain the microstructural information regarding the morphology, particle size, Al/Cu interfacial structure, and the distribution of Al deposits on Cu electrodes.

3. Results and Discussion

3.1 XRD Analysis

Typical XRD patterns of the Al deposit samples are shown in Fig. 2, which were collected at 100 ^{o}C on Cu electrodes polished by 320, 600, 800, 1200 grits SiC sandpapers and mirror polishing procedure. To avoid the X-ray signal from Cu electrode, the Al deposits were removed and collected from the Cu electrodes using a plastic scrap board before XRD analysis. As indicated in Fig. 2, phase-pure and well-crystallized Al deposits (JCPDS #04-0787) were obtained at 100 ^{o}C using Cu electrodes with varied surface roughness, and no other impurity phases were observed. In addition, it can be noted that the XRD peak intensity of Al deposits decreases with decreasing surface roughness of Cu electrodes (from 543.1$\pm$59.7 nm for 320G Cu electrode to 23.3±4.8 nm for mirror Cu electrode), owing to the decreasing amount of Al deposits, which is consistent with the results from the plan-view SEM analysis below. Under other deposition temperatures (80 ^{o}C, 90 ^{o}C, and 110-140 ^{o}C), the XRD patterns are similar except the crystallinity of Al deposits.

3.2 Effect of Deposition Temperature

Fig. 3 shows the time-dependent changes of the current density during Al electrodeposition at different deposition temperatures from 80 ^{o}C to 140 ^{o}C. It can be observed that as the deposition

temperature increases, the current density increases significantly from 167.5 A/m^2 at 80 ^{o}C to 773.8 A/m^2 at 140 ^{o}C (~360% increase). According to Goux et al (Goux et al., 2005), they investigated the deposition temperature effect on the current density for ZnO electrodeposition from 22 to 50 ^{o}C at a stirring rate of 300 rpm and from 50 to 89 ^{o}C at a stirring rate of 500 rpm, and concluded that the higher deposition temperature accelerates the formation and growth of ZnO. Wang et al (Wang et al., 2012) studied the temperature effect for electrodeposition of $Ni(OH)_2$ and demonstrated that the deposition temperature significantly impacts the crystalline structure, morphology, specific surface area and electrochemical characteristics like the proton diffuse coefficient. Using the same ionic liquid electrolyte ($AlCl_3$+BMIC), Kamavaram (Kamavaram, 2004) reported that the diffusion of $Al_2Cl_7^-$ ions in BMIC can be promoted at higher deposition temperature. In summary, Al electrodeposition reaction that takes place at the Cu electrode/ionic liquid electrolyte interfacial region involves both mass transfer and charge transfer steps. The final rate of reduction ($4Al_2Cl_7^- + 3e^- = Al + 7AlCl_4^-$), and hence the current density, is determined by the slower one of these two steps. The main reason that contributes to the improved current density at higher deposition temperature can be summarized as: the increasing deposition temperature instigates a decreased viscosity of $AlCl_3$-BMIC ionic liquid electrolyte (Fannin et al., 1984), which further enhances the diffusion (mass transfer) of reducible $Al_2Cl_7^-$ ions towards the Cu electrode. The faster diffusion reduces the concentration difference (polarization) and finally promotes the electrode reaction rate.

Fig. 4 shows the current efficiency and energy consumption at different deposition temperatures from 80 ^{o}C to 140 ^{o}C. The increasing deposition temperature leads to a significant build-up of current efficiency from 72% at 80 ^{o}C to 96% at 100 ^{o}C, which owes to the accelerated diffusion of $Al_2Cl_7^-$. Both Abbott (Abbott et al., 2005; Abbott and McKenzie, 2006)

and Kamavaram (Kamavaram, 2004) demonstrated the limited effect of applied potential on the reaction rate: when applied potential is too high, the fast diffusion or migration of $Al_2Cl_7^-$ limits the reaction rate. That means the increase in deposition temperature augments the diffusion or migration of reducible $Al_2Cl_7^-$ ions towards Cu electrode which increases the deposition rate of Al. In addition, the accelerated Al electrodeposition inhibits the side reactions such as dissociation of organic cations and re-dissolution of Al deposits. As a result, the current efficiency increases, and energy consumption decreases as shown in Fig. 4. However, above 100 ^oC, only slight change in the current efficiency was observed. So, for the following study of surface roughness effect for Cu electrode, the deposition temperature was kept at 100 ^oC for all remaining experiments.

The cross-section SEM images of Al deposits prepared at different deposition temperatures from 80 ^oC to 140 ^oC are shown in Fig. 5. Fig. 5 presents the SEM images of Al deposits at (a) 80 ^oC, (b) 100 ^oC, (c) 120 ^oC and 140 ^oC. It is obviously seen that the dendrite structure of Al deposits changes from tree-like to leaf-like (plate-like) structure with the increasing deposition temperature. Furthermore, from the high magnification SEM images. These microstructural transforms are attributed to the promoted growth of deposited Al at higher deposition temperature, which is consistent with the changes in current density. For instance, Raeissi et al (Raeissi et al., 2003) revealed that the change in morphology of deposited zinc (Zn) was related to the nucleation and growth of crystalline under different deposition conditions including temperature, pH and current density. Aghazadeh et al (Aghazadeh et al., 2013) reported that the bath liquid temperature for Y_2O_3 electrodeposition had a critical role on the crystal structure and morphology of products, while the morphologies of Y_2O_3 deposited at 10, 25, 40 and 80 ^oC were completely different. Li (Li et al., 2014) studied the deposition temperature effect on the

morphology for Ni electrodeposition in $BMIMBF_4$ ionic liquid and observed that the particles growth and crystalline structure changes with varying deposition temperature. In this study, the increasing deposition temperature promotes the diffusion of $Al_2Cl_7^-$ and accelerates the nucleation and growth of Al deposits.

To explain this effect, the Eq. [7], Stokes-Einstein equation, was used here,

$$D = \frac{kT}{Br\eta} \quad [7]$$

Where D is the diffusion coefficient, k is the Boltzmann's constant, T is the absolute temperature, B is the numerical coefficient, r is the radius of the moving $Al_2Cl_7^-$ and η is the viscosity of the $AlCl_3$-BMIC ionic liquid electrolyte. Taking the factors into consideration of Fannin et al's conclusion (Fannin et al., 1984) and Eq. [7], the increasing deposition temperature can decrease the viscosity (η) of $AlCl_3$-BMIC ionic liquid electrolyte and further increases the diffusion coefficient (D), which is positively correlated to the flux of substance. As a result, the flux of $AlCl_4^-$ and $Al_2Cl_7^-$ is enhanced at higher electrolyte temperature, leading to the higher concentration of $Al_2Cl_7^-$ at the interface of Cu/$AlCl_3$-BMIC ionic liquid electrolyte. Finally, the higher concentration of $Al_2Cl_7^-$ accelerates the Al deposition on the Cu electrode, providing higher current density as shown in Fig. 3. In addition, the higher electrolyte temperature promotes the nucleation and growth of Al deposits, which is consistent with the SEM analysis (Fig. 5). Table 1 summarizes the experimental variables and measured current density, current efficiency, and energy consumption for the study of deposition temperature effect.

3.2 Effect of Cu Electrode Surface Roughness

Fig. 6 presents the plan-view SEM images of polished Cu electrodes by 320, 600, 800, 1200 grits SiC sandpapers and mirror polished procedure. Table 2 summarizes the experimental

variables and measured current density, current efficiency, and energy consumption for the study of Cu surface roughness effect. The average surface roughness (Ra, also called mean roughness) is defined as the arithmetic average of the absolute heights of Cu electrodes, offering a good general description of the surface height variation after different polishing conditions. The depth profiles of the polished Cu electrodes are shown in Fig. 7. Fig. 7 indicates that the depth of the groove features on Cu electrodes becomes smaller from 320G Cu to mirror Cu, which is consistent with the results of Fig. 6 and Table 2. Combined the results of Figs 1, 6, 7 and Table 2, it is concluded that the surface roughness (Ra) of Cu electrodes becomes smaller after polishing with the larger number SiC grit sandpaper, and changes to the smallest value at 23.3±4.8 nm after the mirror polishing process. This is because the grit size of SiC sandpaper is inversely related to the particle size of SiC abrasive. A larger grit number sandpaper has finer surface and the polished Cu electrodes become smoother (lower surface roughness).

Fig. 8 shows the cross-section SEM images of Al deposits on Cu electrodes with different surface roughness. Shown in Fig. 8 (a~d), there are large amounts of dendrite structure observed on Cu electrodes with larger surface roughness, but the relative amount of the dendrite structure seems to decline with the decreasing surface roughness of Cu electrodes (note that these SEM images are not in the same magnification), and the dendrite structure finally disappears and Al deposits become flat plate-like morphology on mirror Cu electrode shown in Fig. 8 (e). In addition, it is exhibited in high magnification images that the deposited Al on Cu electrodes with low surface roughness has larger particle size and layer or plate-like morphology, which indicates that the growth of Al grains is much faster along certain Al crystal planes on smoother Cu surface, possibly due to lesser physical groove barriers on these surfaces.

Fig. 9 exhibits the plan-view SEM images of deposited Al on Cu electrodes with different

surface roughness. From Fig. 9 (a~c), it can be noted that the Al deposition density is much higher on rougher surface of Cu electrodes (Fig. 9 a-c). In contrast, the Al deposits on 1200G Cu (Fig. 9 d) and mirror Cu (Fig. 9 e) are sparsely distributed and in some locations the Cu electrode is even exposed, indicating no Al deposition in these areas. This is due to either weak interfacial adhesion between deposited Al and Cu electrode or lack of nucleation and growth sites on smoother Cu electrodes. And the trend of the decreased deposition density and structural evolution from dendrite to plate-like structure on smoother Cu electrodes is consistent with the cross-section SEM analysis displayed in Fig. 8.

The SEM images and EDS results of the Al deposits on the 320G and 1200G SiC sandpapers polished Cu electrodes are compared in Fig. 10. For the deposited Al on 320G Cu, it has a much smaller particle size than that of Al on 1200G Cu. And the Al deposits on 320G Cu appear a polyhedral morphology, while the Al deposits on 1200G Cu present 2D-like thin layer structure. However, the EDS results show that both their chemical composition is essential pure Al with very small amount of oxygen, indicating that no apparent oxidation of Al occurs during the drying and posttreatments. According to Vilain and Ebothe (Vilain et al., 1996), the surface roughness of deposition electrode can be associated with an increase in the grain size of Ni-Co alloy deposits and influence the domain wall. Huang et al (Huang et al., 2009) studied the effect of electrode surface roughness on nanoarchitectures of Au particles from directed electrodeposition, and discovered the growth of Au followed a diffusion-controlled mechanism. Their results showed that the thickness of diffusion layer and the 3D-shape of Au particles are completely different. In other words, the surface roughness of the Cu electrode is critical to the nucleation and growth processes of Al during electrodeposition, which determines the final particle size and morphology.

The main stage of the electrodeposition (or "electrocrystallization") process is continuous incorporation of ad-atoms or ad-molecules at the expanding periphery of the nucleation centers (Bewick et al., 1962). According to Bhatt et al's work (Bhatt et al., 2007) on the electrodeposition of lead with ionic liquid, the initial nucleation during electrodeposition influences the further growth of crystals and can be divided into two main types: instantaneous and progressive, which are determined by the diffusion-controlled mass transfer of related ions. Instantaneous nucleation describes the process where the nuclei are formed at the beginning of the electric pulse and progressive nucleation depicts the process where the nuclei are continuously formed during the crystal growth, which has been theoretically and experimentally studied by Scharifker and Hills (Scharifker and Hills, 1983). According to Pradhan and Reddy (Pradhan and Reddy, 2014), the Al electrodeposition from $AlCl_3$-BMIC electrolytes precedes via instantaneous nucleation process.

Surface roughness of deposition electrode has been known to affect nucleation of deposited species during electrodeposition. The process of scratching electrode surface using sandpapers results in variable surface roughness and irregularities such as grooves and pits (Bi et al., 2017). According to Fletcher (Fletcher, 1958), the nucleation process is very sensitive to changes of interfacial energy, which is indirectly related to the surface roughness of electrode. Furthermore, in Turnbull' study (Turnbull, 1950), the active role of surface irregularities on rough surface nucleation is well described by the heterogeneous classical nucleation theory through a simple geometric argument: it is clearly calculated that the concave cavity, which can be created by scratching, reduces the volume of critical nucleus further than a flat or a convex surface due to the different contact angles between embryo and substrate surface. A large amount of nucleus on rough surface promotes the formation of dendrite structure, which is consistent with the SEM

observation.

In our case, the roughness effect on electrodeposition can be explained with crystal nucleation and contact angle. According to previous study (Ohara and Reid, 1973), roughness enhances surface wettability and influences contact angle, which are the major parameters that affect heterogeneous nucleation. The relationship between the rate of primary heterogeneous nucleation J and nucleation energy is given by (Keysar et al., 1994)

$$J = A * exp\ (\frac{-(\Delta G_c)_{het}}{kT}) \quad [8]$$

where $(\Delta G_c)_{het}$ is the free energy change required to nucleate a stable, initial-size crystallite; A is the frequency factor; k is the Bolzman constant; and T is the absolute temperature. Moreover, the extent of this free energy barrier depends on the contact angle θ of the crystallite on the substrate surface and supersaturation level S.

$$-(\Delta G_c)_{het} = \emptyset * (\Delta G_c)_{hom} = \emptyset * \frac{B}{(\ln S)^2} \quad [9]$$

where $(\Delta G_c)_{hom}$ is the maximum energy barrier for homogeneous nucleation; the fractional reduction of the energy barrier, ∅, can be described as a function of the contact angle θ as follows, when the nucleus on flat surface is cap-shaped structure (Kashchiev, 2000):

$$\emptyset = \frac{(2+\cos\theta)*(1-\cos\theta)^2}{4} \quad [10]$$

It can be observed that, the reduction factor ∅ varies from 1 (no energy reduction) to 0 (no energy barrier) when the contact angle θ decreases from 180° (non-wetting) to 0° (full-wetting). That means the decreasing contact angle promotes the nucleation on the substrate surface and the number of nuclei sites increases. From geometrical consideration, Wenzel (Wenzel, 1936) showed that the contact angle θ' on a rough surface is associated with the contact angle θ on a smooth surface by "roughness factor" r

$$r = \frac{\text{Ture Surface Area}}{\text{Apparent Planar Area}} = \frac{\cos\theta_r}{\cos\theta} \quad [11]$$

Generally, r is larger than 1 for rough surface, which means that the rough surface will reduce the contact angle for wetting condition ($\theta < 90°$). Considering about the electrodeposition process and materials used in this study, the result of deposition on rough surface is that rougher surface increases the nucleation rate by reducing the contact angle, leading to larger amount of nuclei sites, higher local concentration of Al species, and more dendrite structure.

To better understand the influence of the surface roughness of Cu electrodes on the nucleation and growth of deposited Al crystals, Fig. 11 present the schematic drawing of possible Al electrodeposition process and growth mechanisms on Cu electrode with different surface roughness. Shown in Fig. 11, for the rough surface (top row), the number of individual heterogeneous nucleation site of Al is much higher due to the narrow groove width. And these surface feature limits the direction of Al mass flow and dilution, leading to the perpendicular growth preference on rough surface due to the inhomogeneous concentration distribution. As a result, the size of Al nuclei is smaller, and the growth direction of Al prefers perpendicular to the Cu electrode plane. The high concentration of $Al_2Cl_7^-$ ions within the grooves promotes the growth of 1D dendrite structure. In addition, the smaller particle size of Al is due to the large amount of nucleation sites, which bring more grain boundaries and block the grain growth. For the slightly rougher surface (middle row), the groove interspace becomes larger, so there are more $Al_2Cl_7^-$ ions or Al atoms for nucleation and growth and the contact angle at the liquid/solid interface changes near to flat surface. Although the space for Al nuclei within the groove structure increases, the crystals still grow along the perpendicular orientation of Cu electrode. The dendrite structure presents better crystallinity with larger grain size. For the smooth surface (bottom row), owing to the larger space compared to the rough surface, the Al nuclei can “absorb”

free Al species from different directions and grow without concentration distribution and space limitation, so there is no observed 1D dendrite structure of deposited Al on mirror Cu electrode.

Fig. 12 shows the time-dependent current density during Al electrodeposition on Cu electrodes with different surface roughness and Fig. 13 describes the effect of surface roughness on current density. It can be observed that as the surface roughness of Cu electrode decreases, the current density increases. We hypothesize that the decreasing surface roughness of Cu electrode prevents the formation of large amounts of Al nuclei, which inhibits the formation of dendrite structure and results in higher current density. Fig. 14 shows the current efficiency and energy consumption of Al electrodeposition on Cu electrodes with different surface roughness. The decreasing surface roughness of Cu electrodes leads to the decrease of current efficiency, which owes to the reduced adhesion force. Loglio et al (Loglio et al., 2004) studied the formation of ternary Cd-ZnS-Se from electrodeposition. They observed low Zn coverage during the electrodeposition and explained this with partial Zn re-dissolution. In our case, the exposed Cu electrode and reduced current efficiency can be explained that the smooth surface provides weaker adhesion force between deposited Al and Cu electrodes compared to the Al deposits on rougher surface (Keysar et al., 1994).

4. Conclusion

In this work, the effects of deposition temperature and surface roughness of Cu electrodes on Al electrodeposition using $AlCl_3$+BMIC ionic liquid electrolyte were studied. For the effect of deposition temperature, it is discovered that higher deposition temperature promotes the diffusion of $Al_2Cl_7^-$ ions, which leads to the increase of the current density and Al electrodeposition. And higher deposition temperature also accelerates the growth of Al crystals,

producing larger particle size and significant changes of structure from dendrite to leaf or plate-like structure. For the surface roughness effect of Cu electrode, it is found that the smoother surface of Cu electrodes reduces the orientation growth of Al crystals, resulting in less dendrite structure and larger particle size. However, the current efficiency is lower on smoother surface possibly due to lack of adhesion force. Therefore, smoother surface of Cu electrodes, lesser dendrite structure.

Acknowledgement

This work is supported by AlChE-DOE RAPID project (DE-EE0007888). This project also receives partial financial support from the ACIPCO, Alabama Water Institute, Alabama Transportation Institute, and The University of Alabama Research Grants Committee (RGC). The use of TEM facilities at the Central Analytical Facility at The University of Alabama is gratefully acknowledged.

Reference

Abbott, A.P., Capper, G., Davies, D.L., Rasheed, R.K., Shikotra, P., 2005. Selective extraction of metals from mixed oxide matrixes using choline-based ionic liquids. Inorg. Chem 44(19), 6497-6499.

Abbott, A.P., McKenzie, K.J., 2006. Application of ionic liquids to the electrodeposition of metals. Phys. Chem. Chem. Phys. 8(37), 4265-4279.

Aghazadeh, M., Malek Barmi, A.-A., Mohammad Shiri, H., Sedaghat, S., 2013. Cathodic electrodeposition of $Y(OH)_3$ and Y_2O_3 nanostructures from chloride bath. Part II: Effect of the bath temperature on the crystal structure, composition and morphology. Ceram. Int 39(2), 1045-1055.

Bewick, A., Fleischmann, M., Thirsk, H.R., 1962. Kinetics of the electrocrystallization of thin films of calomel. J. Chem. Soc. Faraday Trans. 58(0), 2200-2216.

Bhatt, A.I., Bond, A.M., Zhang, J., 2007. Electrodeposition of lead on glassy carbon and mercury film electrodes from a distillable room temperature ionic liquid, DIMCARB. J. Solid State Electrochem. 11(12), 1593-1603.

Bi, Y., Cao, B., Li, T., 2017. Enhanced heterogeneous ice nucleation by special surface geometry. Nat. Commun. 8(1), 15372.

Fannin, A.A., Floreani, D.A., King, L.A., Landers, J.S., Piersma, B.J., Stech, D.J., Vaughn, R.L., Wilkes, J.S., Williams, J.L., 1984. Properties of 1,3-dialkylimidazolium chloride-aluminum chloride ionic liquids. 2. Phase transitions, densities, electrical conductivities, and viscosities. J. Phys. Chem. 88(12), 2614-2621.

Fletcher, N.H., 1958. Size effect in heterogeneous nucleation. The Journal of Chemical Physics 29(3), 572-576.

Gomes, A., da Silva Pereira, M.I., 2006. Zn electrodeposition in the presence of surfactants: Part I. Voltammetric and structural studies. Electrochim. Acta 52(3), 863-871.

Goux, A., Pauporté, T., Chivot, J., Lincot, D., 2005. Temperature effects on ZnO electrodeposition. Electrochim. Acta 50(11), 2239-2248.

Huan, S., Wang, Y., Peng, J., Di, Y., Li, B., Zhang, L., 2020. Recovery of aluminum from waste aluminum alloy by low-temperature molten salt electrolysis. Miner. Eng. 154, 106386.

Huang, X.-J., Yarimaga, O., Kim, J.-H., Choi, Y.-K., 2009. Substrate surface roughness-dependent 3-D complex nanoarchitectures of gold particles from directed electrodeposition. J. Mater. Chem. 19(4), 478-483.

Kamavaram, V., 2004. Ph.D. Dissertation. The University of Alabama，Tuscaloosa.

Kamavaram, V., Mantha, D., Reddy, R.G., 2005. Recycling of aluminum metal matrix composite using ionic liquids:: Effect of process variables on current efficiency and deposit characteristics. Electrochimica Acta 50(16), 3286-3295.

Kashchiev, D., 2000. Chapter 9 - Master equation, in: Kashchiev, D. (Ed.) Nucleation. Butterworth-Heinemann, Oxford, pp. 115-135.

Keysar, S., Semiat, R., Hasson, D., Yahalom, J., 1994. Effect of Surface Roughness on the Morphology of Calcite Crystallizing on Mild Steel. J. Colloid Interface Sci. 162(2), 311-319.

Kuma, C., Sato, K., Hanaoka, Y., Matsui, I., Takigawa, Y., Uesugi, T., Higashi, K., 2019. Reduction of impurity contents in aluminum plates electrodeposited from a dimethylsulfone-aluminum chloride bath. J. Alloys Compd. 783, 919-926.

Li, M., Wang, Z., Reddy, R.G., 2014. Electrodeposition of nickel in 1-butyl-3-methylimidazolium tetrafluoroborate ionic liquids. J. Electrochem. Soc. 161(4), D150-D153.
Loglio, F., Innocenti, M., Pezzatini, G., Foresti, M.L., 2004. Ternary cadmium and zinc sulfides and selenides: electrodeposition by ECALE and electrochemical characterization. J. Electroanal. Chem. 562(1), 117-125.
Ohara, M., Reid, R.C., 1973. Modeling crystal growth rates from solution. Prentice-Hall.
Popov, K.I., Djukić, L.M., Pavlović, M.G., Maksimović, M.D., 1979. The critical overpotential for copper dendrite formation. J. Appl. Electrochem. 9(4), 527-531.
Pradhan, D., Mantha, D., Reddy, R.G., 2009. The effect of electrode surface modification and cathode overpotential on deposit characteristics in aluminum electrorefining using EMIC–$AlCl_3$ ionic liquid electrolyte. Electrochim. Acta 54(26), 6661-6667.
Pradhan, D., Reddy, R.G., 2012. Dendrite-Free Aluminum Electrodeposition from AlCl3-1-Ethyl-3-Methyl-Imidazolium Chloride Ionic Liquid Electrolytes. Metall. Mater. Trans B 43(3), 519-531.
Pradhan, D., Reddy, R.G., 2014. Mechanistic study of Al electrodeposition from EMIC–AlCl3 and BMIC–AlCl3 electrolytes at low temperature. Mater. Chem. Phys. 143(2), 564-569.
Raeissi, K., Saatchi, A., Golozar, M.A., 2003. Effect of nucleation mode on the morphology and texture of electrodeposited zinc. J. Appl. Electrochem. 33(7), 635-642.
Scharifker, B., Hills, G., 1983. Theoretical and experimental studies of multiple nucleation. Electrochim. Acta 28(7), 879-889.
Turnbull, D., 1950. Kinetics of heterogeneous nucleation. J. Chem. Phys. 18(2), 198-203.
Vilain, S., Ebothe, J., Troyon, M., 1996. Surface roughness and composition effects on the magnetic properties of electrodeposited Ni-Co alloys. J. Magn. Magn. Mater 157-158, 274-275.
Wang, Y.-M., Zhao, D.-D., Zhao, Y.-Q., Xu, C.-L., Li, H.-L., 2012. Effect of electrodeposition temperature on the electrochemical performance of a $Ni(OH)_2$ electrode. RSC Adv. 2(3), 1074-1082.
Wenzel, R.N., 1936. RESISTANCE OF SOLID SURFACES TO WETTING BY WATER. Ind. Eng. Chem. Res. 28(8), 988-994.
Yang, Y., Liu, S., Chi, C., Hao, J., Zhao, J., Xu, Y., Li, Y., 2020. Electrodeposition of a continuous, dendrite-free aluminum film from an ionic liquid and its electrochemical properties. J. Mater. Sci.: Mater. Electron. 31(12), 9937-9945.
Zhang, M., Reddy, R., 2006a. Current density distribution and current efficiency modeling ofaluminum electrodeposition in ionic liquids. Meeting Abstracts MA2005-02(28), 1093.
Zhang, M., Reddy, R., 2006b. Electrical field and current density distribution modeling of aluminum electrodeposition in ionic liquid electrolytes. ECS Trans. 1(16), 47-60.

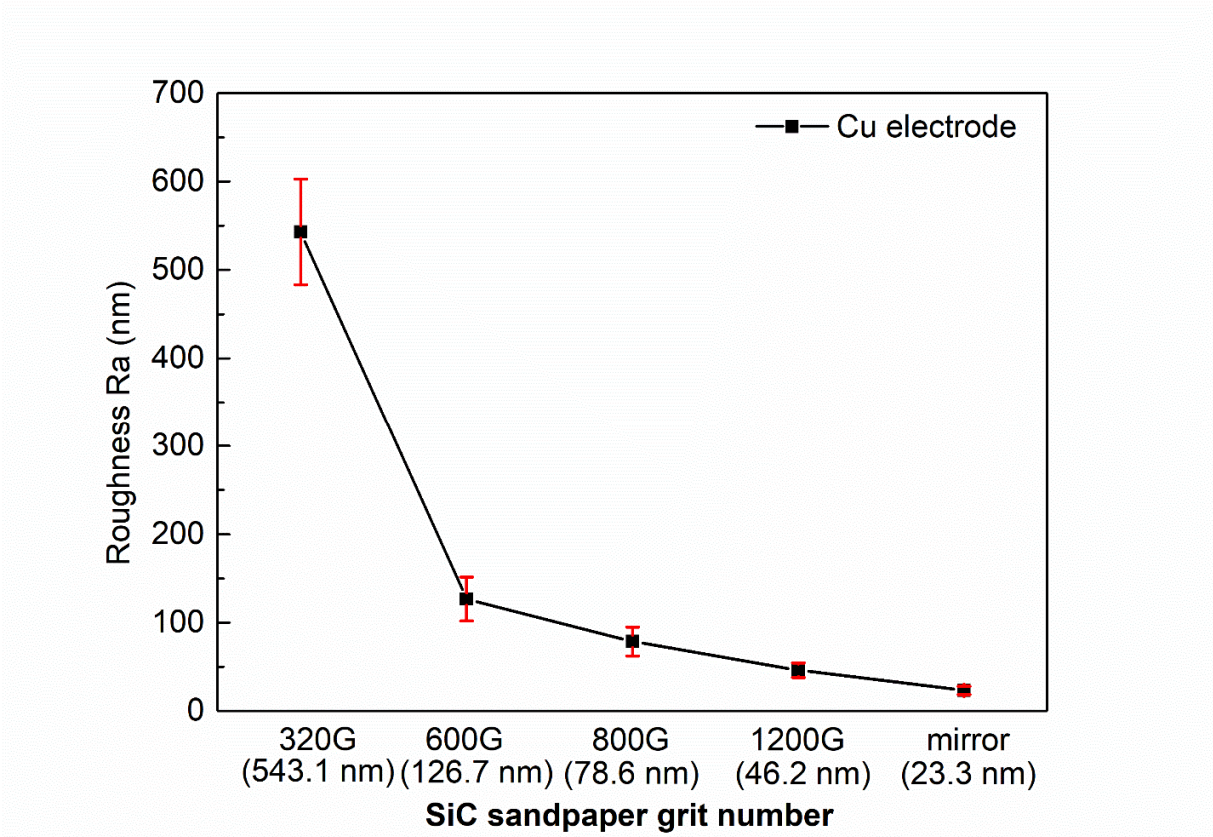

Figure 1. Surface roughness of Cu electrodes polished by 320G (543.1 nm), 400G (126.7 nm), 800G (78.6 nm), 1200G (46.2 nm) SiC sandpapers, and mirror polishing process (23.3 nm).

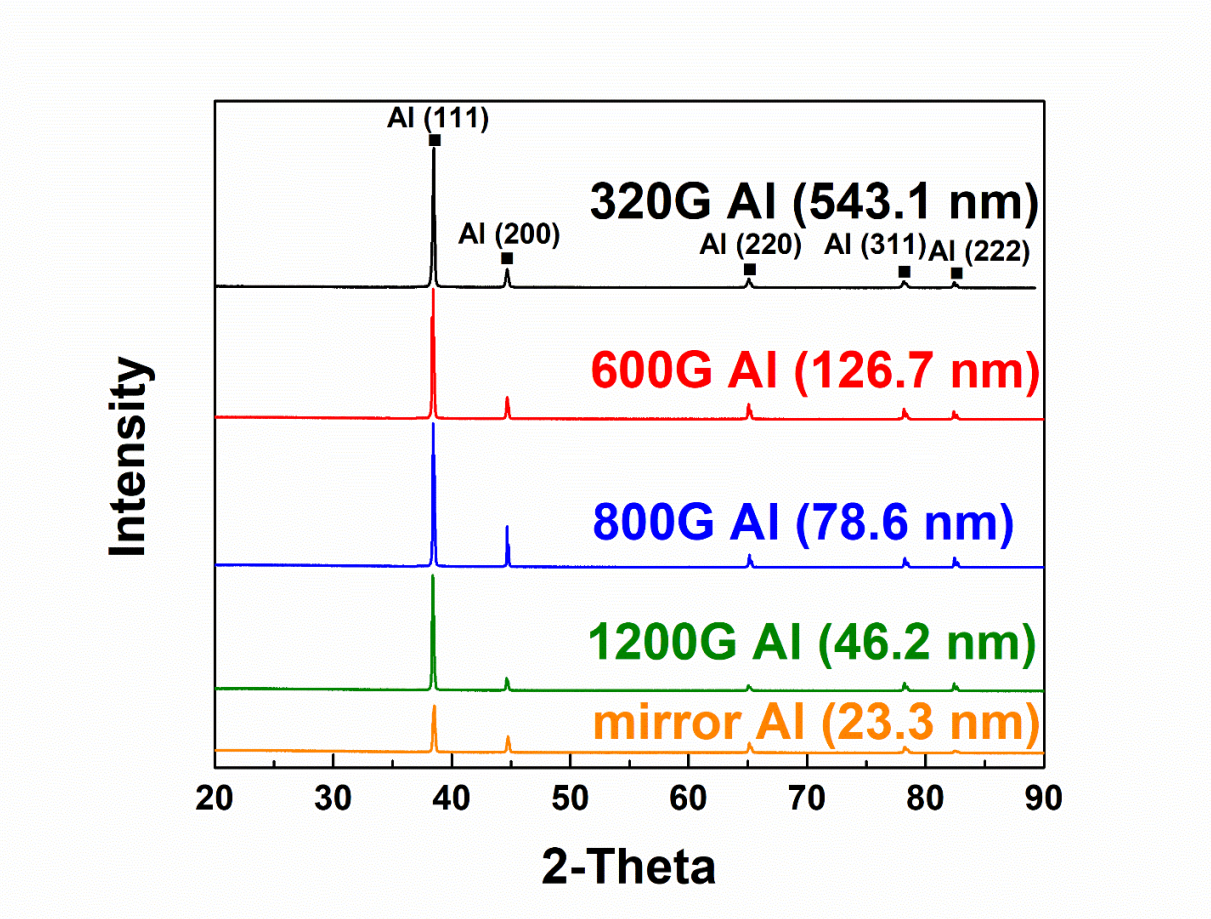

Figure 2. XRD patterns of Al deposits on Cu electrodes polished by 320/600/800/1200 grits SiC sandpapers and mirror polish process.

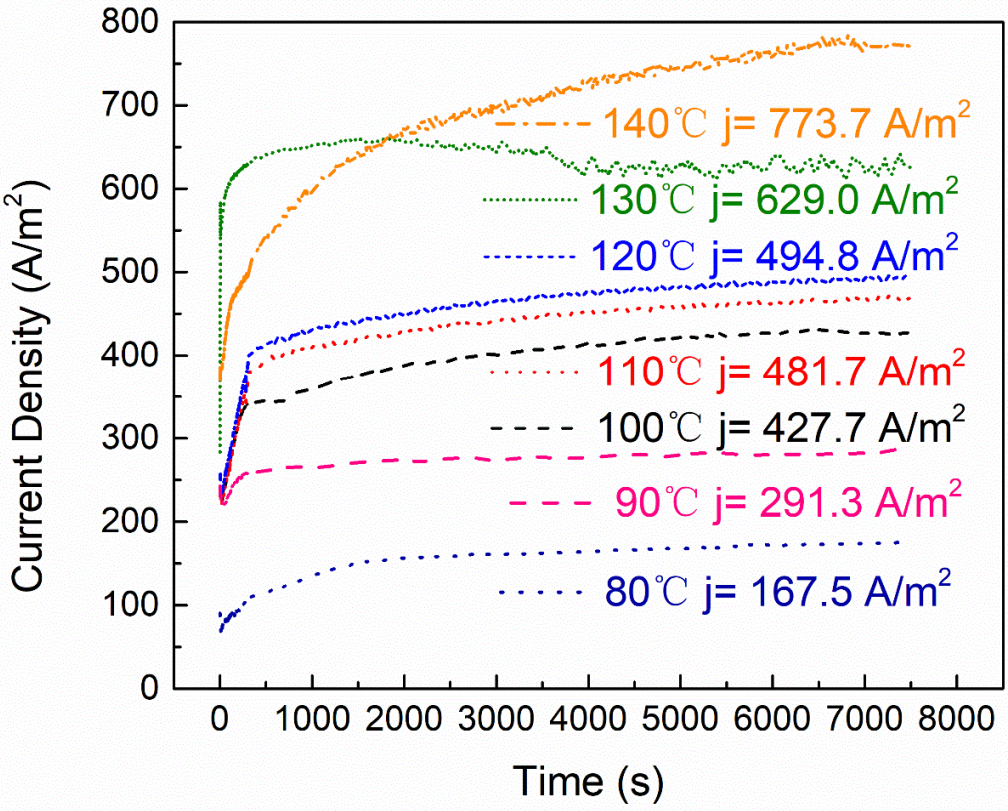

Figure 3. Effect of deposition temperature (electrolyte solution) on the current density from 80 to 140 ºC.

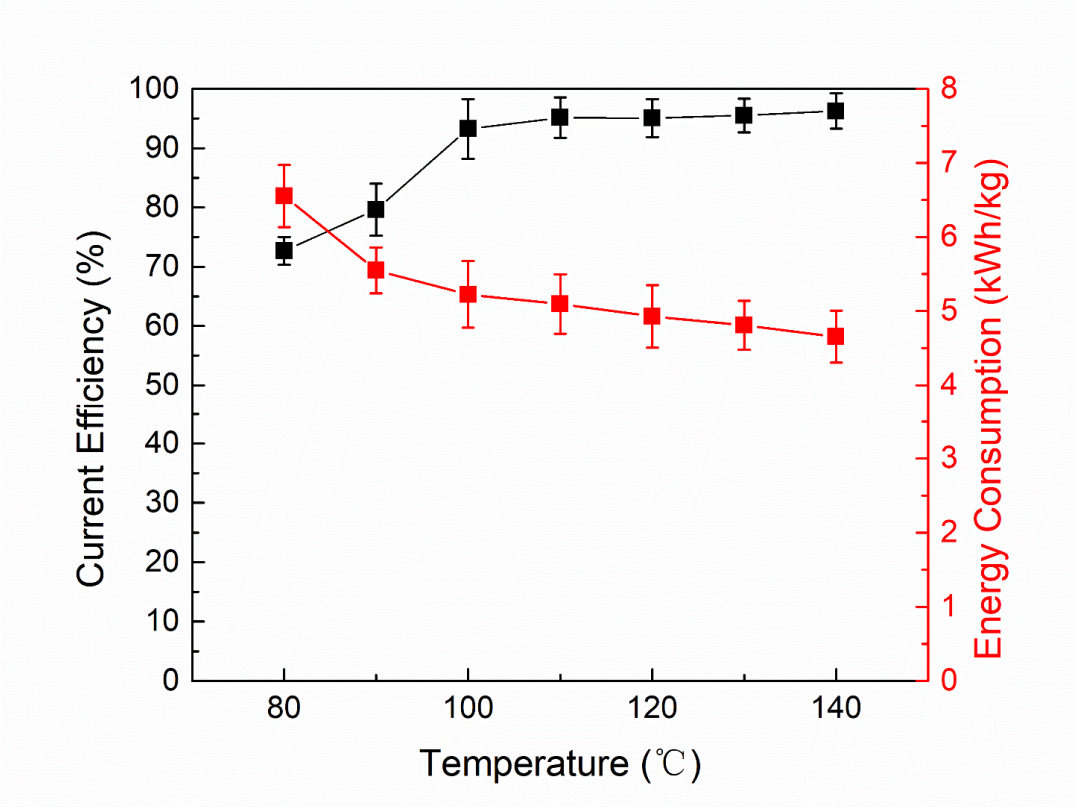

Figure 4. Effect of deposition temperature (electrolyte solution) on the current efficiency and energy consumption from 80 to 140 ºC.

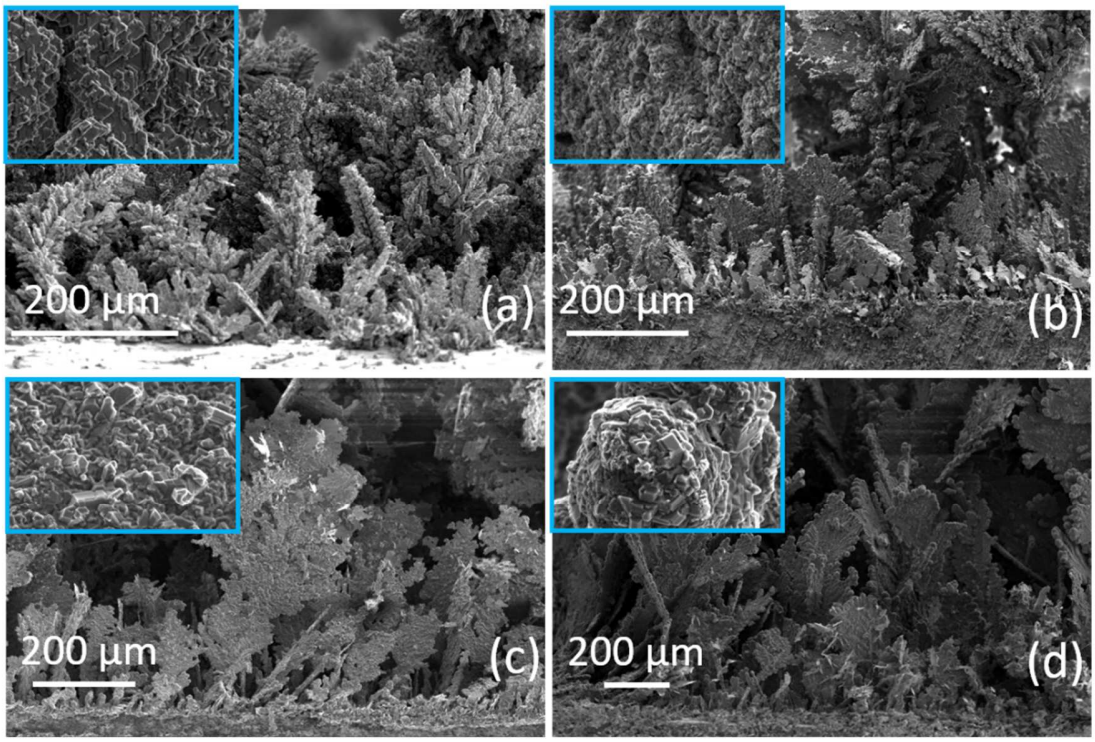

Figure 5. Cross-section SEM images of deposited Al prepared at the deposition temperate (electrolyte solution) at (a) 80 ℃, (b) 100 ℃, (c) 120 ℃ and (d) 140 ℃.

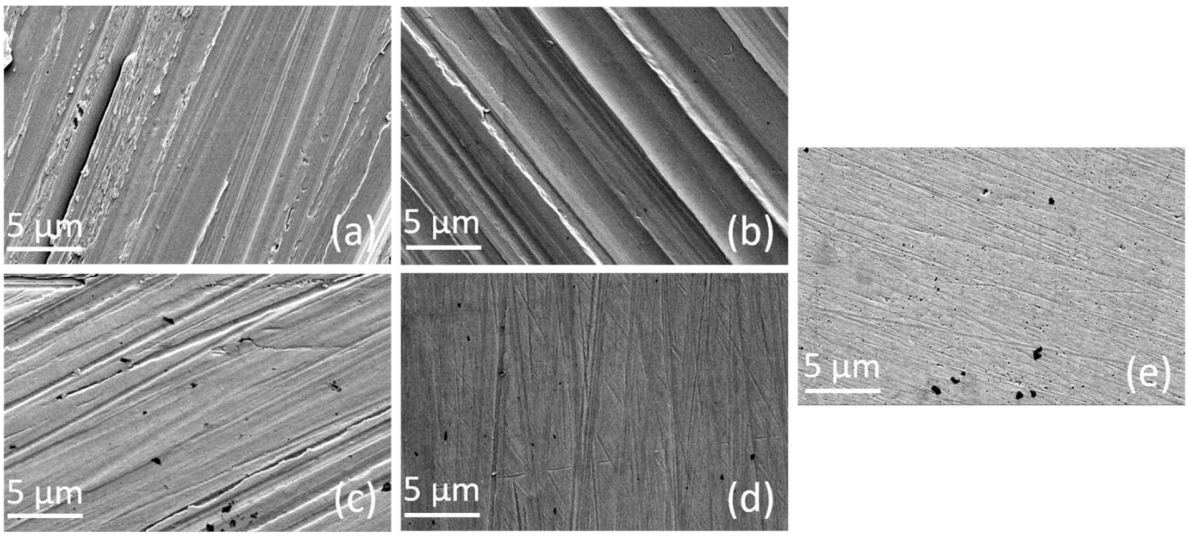

Figure 6. Plan-view SEM images of Cu cathode substrates polished by (a) 320G (543.1 nm), (b) 400G (126.7 nm), (c) 800G (78.6 nm), (d) 1200G SiC (46.2 nm) sandpapers, and (e) mirror polishing process (23.3 nm).

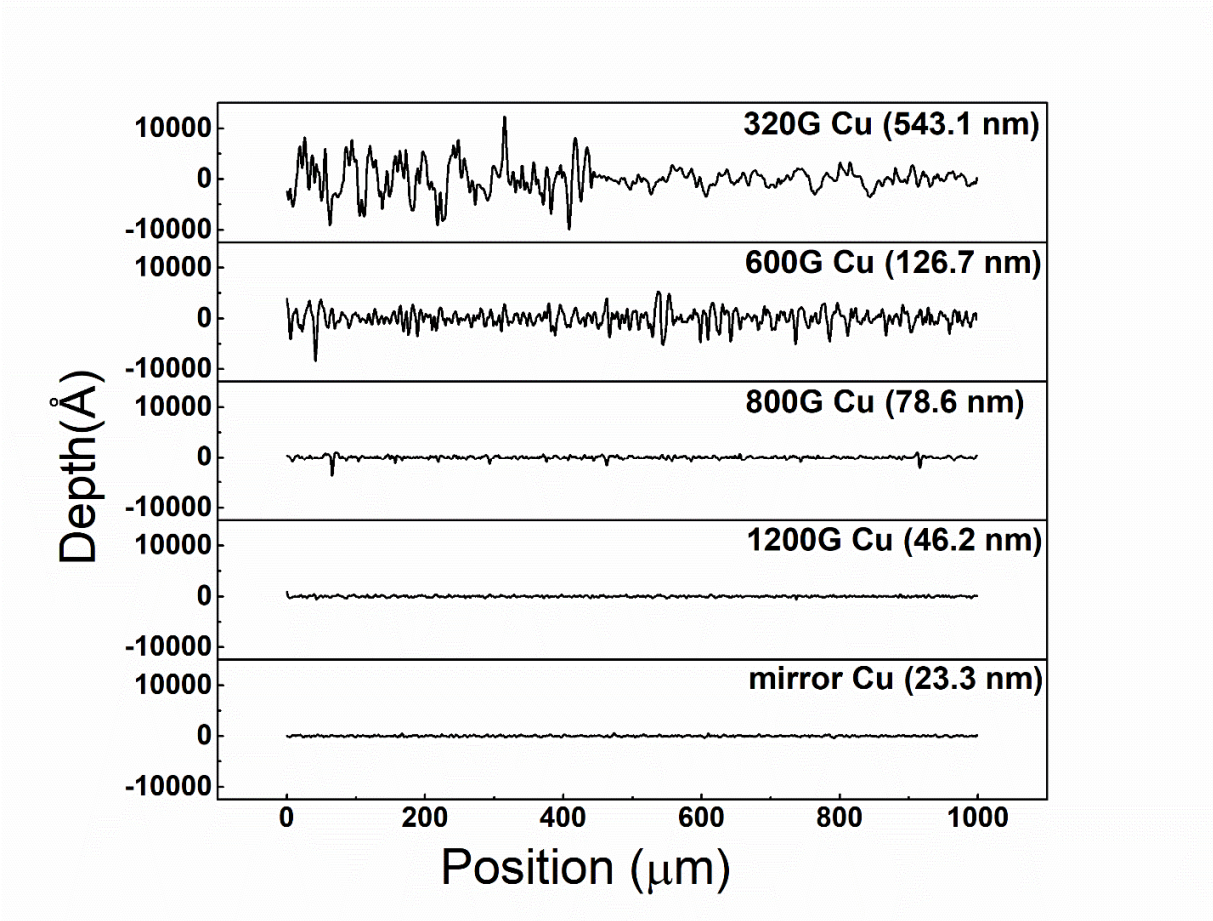

Figure 7. Surface roughness profiles of Cu electrodes after different polish processing.

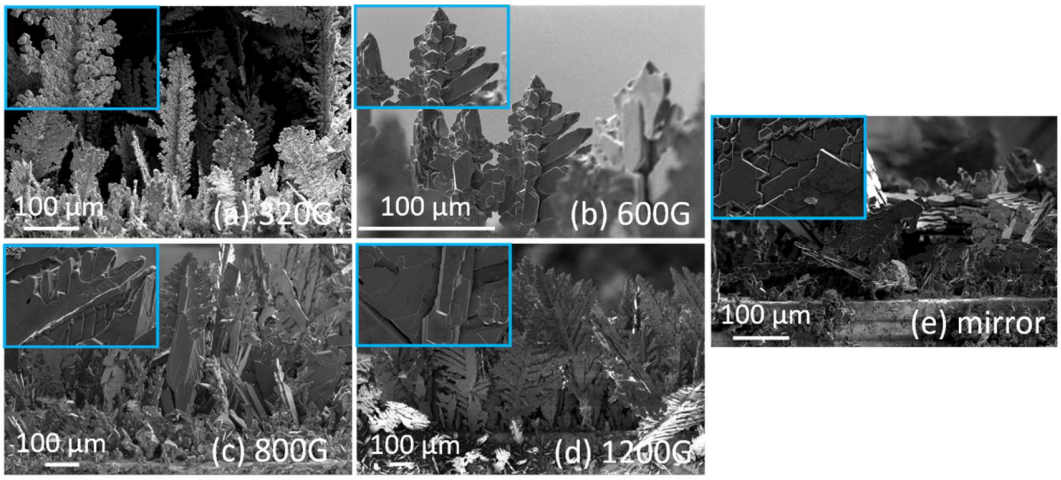

Figure 8. Cross-section SEM images of electrodeposited Al prepared using $AlCl_3$+BMIC ionic liquid electrolyte on (a) 320G (543.1 nm), (b) 400G (126.7 nm), (c) 800G (78.6 nm), (d) 1200G (46.2 nm), (e) mirror polished Cu electrodes (23.3nm).

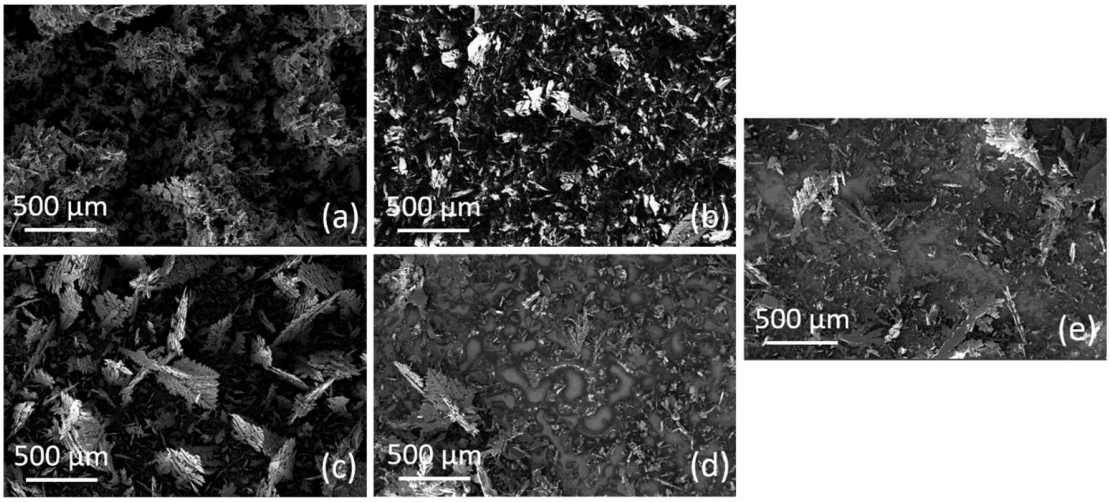

Figure 9. Plan-view SEM images of deposited Al prepared on (a) 320G (543.1 nm), (b) 400G (126.7 nm), (c) 800G (78.6 nm), (d) 1200G (46.2 nm), (e) mirror polished Cu (23.3nm) electrodes.

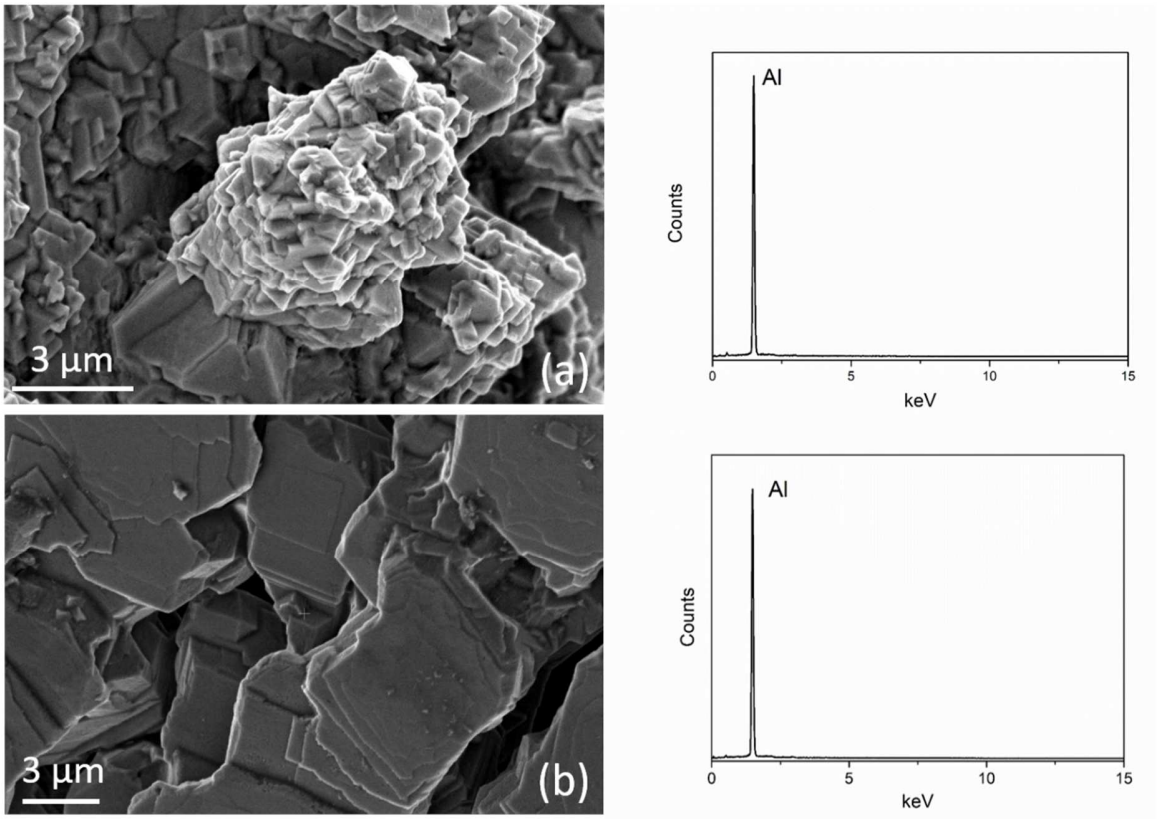

Figure 10. Cross-section SEM images and EDS analysis of deposited Al prepared on (a) 320G (543.1nm) and (b) 1200G Cu electrodes (46.2nm).

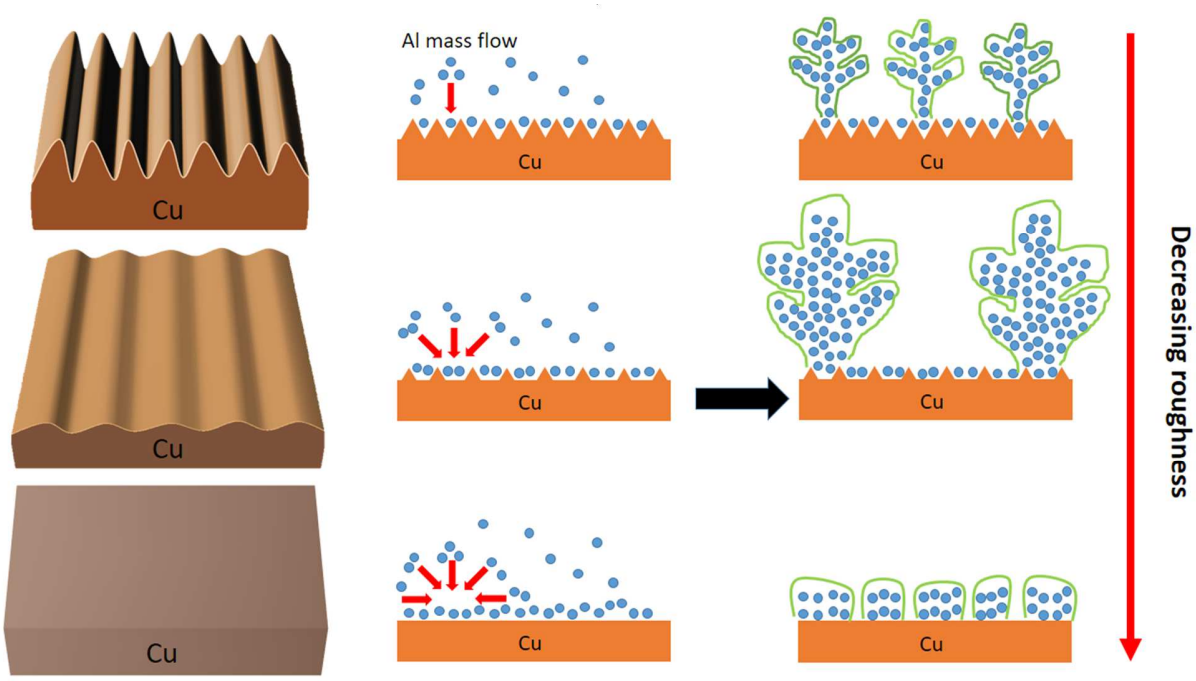

Figure 11. Schematic diagram of surface roughness effect of Cu electrodes on the formation of deposited Al structures.

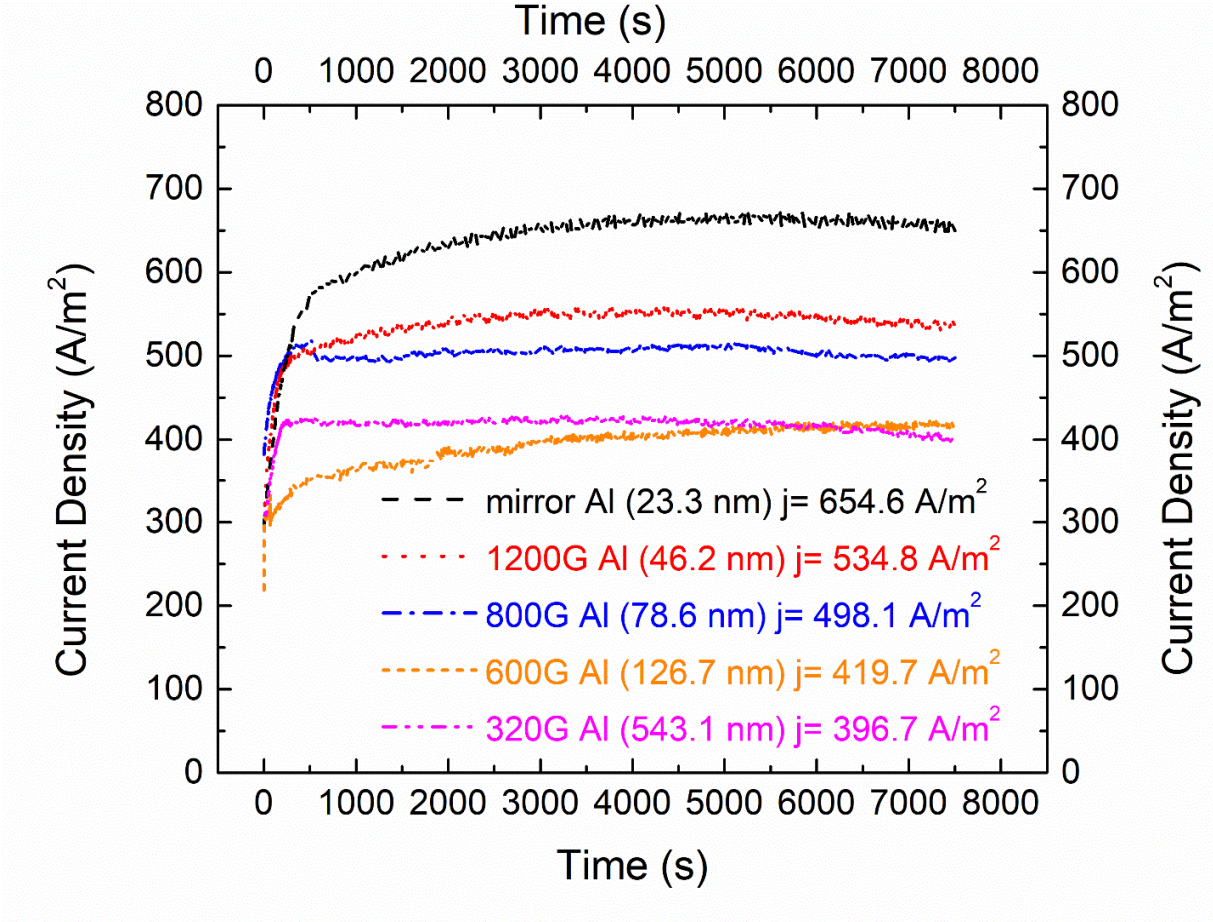

Figure 12. Time-dependent current density during Al electrodeposition on Cu electrodes polished by 320G (543.1 nm), 400G (126.7 nm), 800G (78.6 nm), 1200G (46.2 nm) SiC sandpapers and mirror polishing procedure (23.3 nm).

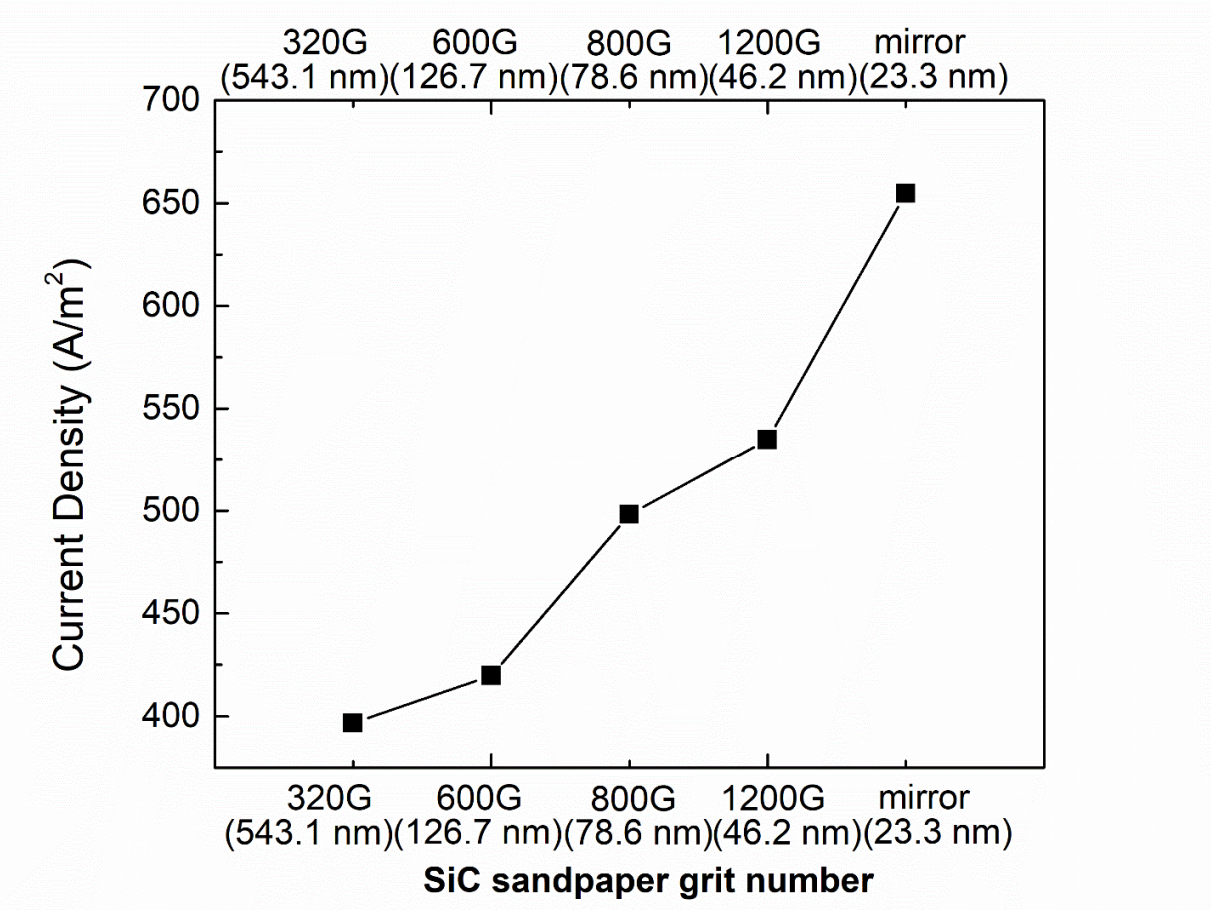

Figure 13. Effect of surface roughness on the current density during Al electrodeposition on Cu electrodes with different roughness.

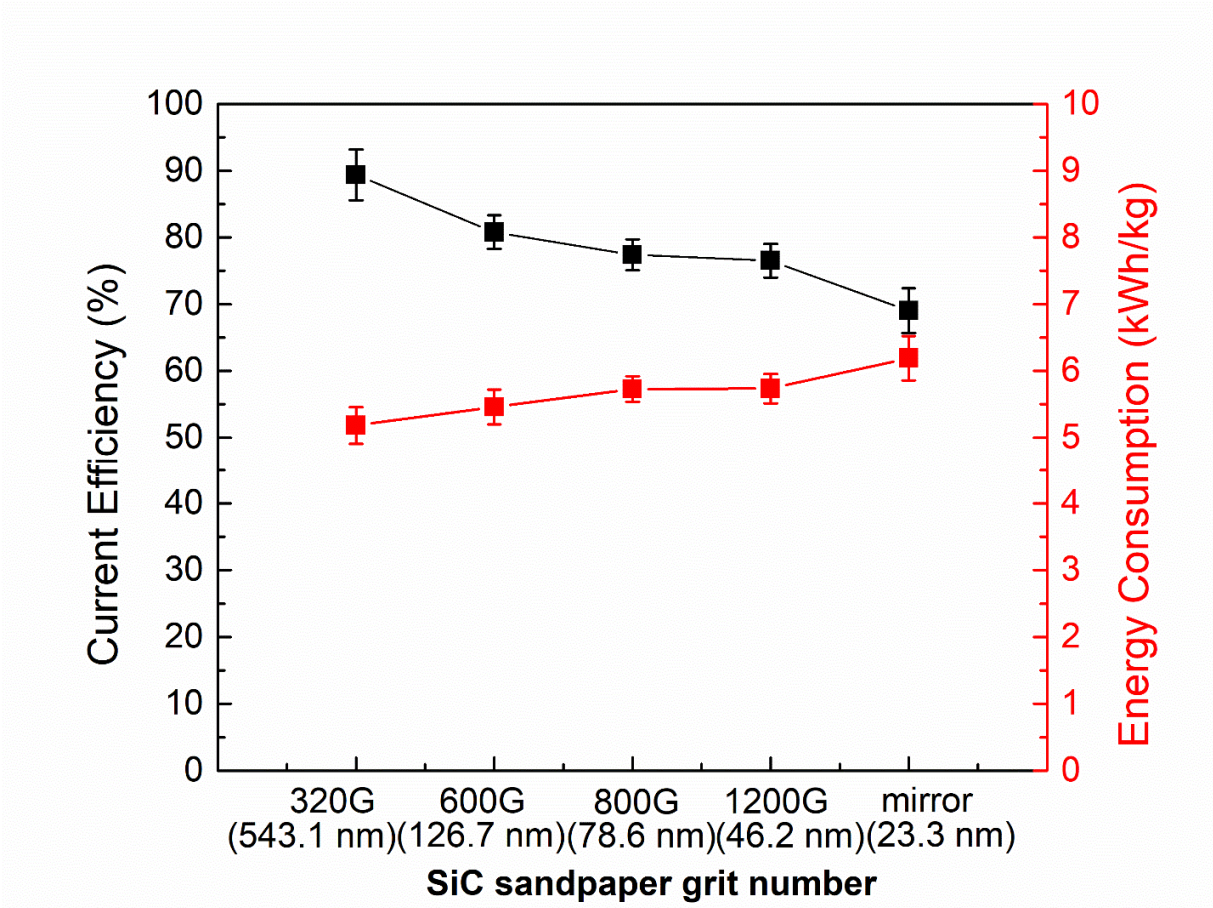

Figure 14. Effect of surface roughness on the current efficiency and energy consumption during Al electrodeposition on Cu electrodes polished by 320G (543.1 nm), 400G (126.7 nm), 800G (78.6 nm), 1200G (46.2 nm) SiC sandpapers and mirror polishing procedure (23.3 nm).

Table 1
The experimental variables and results for the study of deposition temperature effect

Sample	Deposition temperature (°C)	Current density (A/m^2)	Current efficiency (%)	Energy consumption (kWh/kg)
S1	80	167.5	72.7±2.3	6.6±0.4
S2	90	291.3	79.6±4.3	5.6±0.3
S3	100	427.7	93.2±5.1	5.3±0.5
S4	110	481.7	95.1±3.4	5.1±0.4
S5	120	494.8	95.1±3.2	4.9±0.4
S6	130	629.0	95.5±2.8	4.8±0.3
S7	140	773.8	96.3±3.0	4.7±0.3

(Stirring rate: 120 rpm; applied potential 1.5 V; deposition time: 2 h; surface roughness of Cu electrode: 543.1±59.7 nm; electrode distance: 23 mm)

Table 2
The experimental variables and results for the study of substrate surface roughness effect

Sample	Arithmetical average surface roughness of Cu cathode: Ra (nm)	Current density (A/m^2)	Current efficiency (%)	Energy consumption (kWh/kg)
R1	543.1±59.7 (320G)	396.7	89.4±3.8	5.2±0.3
R2	126.7±24.7 (600G)	419.7	80.8±2.5	5.5±0.3
R3	78.6±16.4 (800 G)	498.1	77.4±2.3	5.7±0.2
R4	46.2±8.2 (1200 G)	534.8	76.5±2.5	5.7±0.2
R5	23.3±4.8 (mirror polishing)	654.6	69.0±3.4	6.2±0.3

(Deposition temperature: 100 °C; stirring rate: 120 rpm; applied potential 1.5 V; deposition time: 2 h; electrode distance: 23 mm)

Graphic Abstract